11C-Methionine PET Identifies Astroglia Involvement in Heart–Brain Inflammation Networking After Acute Myocardial Infarction

Pablo Bascuñana[1], Annika Hess[1], Tobias Borchert[1], Yong Wang[2], Kai C. Wollert[2], Frank M. Bengel[1], and James T. Thackeray[1]

[1]Department of Nuclear Medicine, Hannover Medical School, Hannover, Germany; and [2]Molecular and Translational Cardiology, Department of Cardiology and Angiology, Hannover Medical School, Hannover, Germany

Acute myocardial infarction (MI) triggers a local and systemic inflammatory response. We recently showed microglia involvement using translocator protein imaging. Here, we evaluated whether 11C-methionine provides further insight into heart–brain inflammation networking. **Methods:** Male C57BL/6 mice underwent permanent coronary artery ligation followed by 11C-methionine PET at 3 and 7 d ($n = 3$). In subgroups, leukocyte homing was blocked by integrin antibodies ($n = 5$). The cellular substrate for PET signal was identified using brain section immunostaining. **Results:** 11C-methionine uptake (percentage injected dose/cm^3) peaked in the MI region on day 3 (5.9 ± 0.9 vs. 2.4 ± 0.5), decreasing to the control level by day 7 (4.3 ± 0.6). Brain uptake was proportional to cardiac uptake ($r = 0.47$, $P < 0.05$), peaking also on day 3 (2.9 ± 0.4 vs. 2.4 ± 0.3) and returning to baseline on day 7 (2.3 ± 0.4). Integrin blockade reduced uptake at every time point. Immunostaining on day 3 revealed colocalization of the L-type amino acid transporter, with glial fibrillary acidic protein–positive astrocytes but not CD68-positive microglia. **Conclusion:** PET imaging with 11C-methionine specifically identifies an astrocyte component, enabling further dissection of the heart–brain axis in post-MI inflammation.

Key Words: myocardial infarction; inflammation; PET; methionine; astroglia

Patients with cardiovascular disease bear an increased risk of dementia, including Alzheimer disease (1–3). Among various underlying factors, inflammation has been postulated as a link between cardiac injury and neurodegeneration (4–6). Recently, TSPO-targeted whole-body imaging confirmed the presence of concomitant cerebral microglia activation in the acute stages after myocardial infarction (MI) in mice and humans (7). Neuroinflammation, although implicated in the development of Alzheimer dementia (8), is difficult to characterize using conventional blood testing or biopsy. Hence, noninvasive methods to characterize early activation of the heart–brain axis after cardiac damage are desirable.

Several radiotracers have recently been characterized for inflammation imaging, including 11C-methionine, which is routinely used for clinical glioma imaging (9). After MI, 11C-methionine robustly accumulates in proinflammatory leukocytes (10,11). Here, we hypothesize that whole-body 11C-methionine PET may provide insights into heart–brain inflammation networking after MI that are complementary to those obtained previously with translocator protein (TSPO)–targeted imaging.

MATERIALS AND METHODS

Animals

Adult male C57BL/6 mice ($n = 34$; Charles River Laboratories) were housed under standardized environmental conditions with free access to standard laboratory diet and water. All experiments were in accordance with the guidelines of the European Directive 2013/63/EU and German national laws, and with the approval of regional authorities.

Experimental Model

Mice underwent coronary artery ligation ($n = 31$) as described (10). A subgroup of animals ($n = 17$) was treated with an antiintegrin antibody cocktail consisting of anti-CD11a (lymphocyte function–associated antigen-1, clone M17/4), anti-CD11b (macrophage-1 antigen, clone M1/70), and anti CD49 d (very late antigen-4, clone PS/2), injected intraperitoneally 2 h before surgery and again 4 d after MI, as previously described (10). These therapeutic antibodies interfere with leukocyte rolling and extravasation, reducing the recruitment of granulocytes, monocytes, and macrophages to the infarct territory (12). After recovery, 11C-methionine PET was conducted at 3 and 7 d after MI.

Radiochemistry

11C-methionine was synthesized as previously described by S-methylation of S-benzyl-homocysteine (13), yielding high radiochemical purity (>98%) and high specific activity (>10 GBq/μmol).

Small-Animal PET

Whole-body 11C-methionine scans were acquired using an Inveon scanner (Siemens) under isoflurane anesthesia and monitoring of body temperature, breathing frequency, and heart rate. The injected dose was 17.2 ± 5.4 MBq of 11C-methionine. External-source transmission scans were acquired for attenuation correction. Dynamic images (30 min) were reconstructed using a 3-dimensional ordered-subset expectation maximization (2 iterations in 16 subsets), fast maximum a posteriori (18 iterations) algorithm (β = 0.01). The reconstruction resulted in voxel sizes of 0.78 × 0.78 × 0.80 mm.

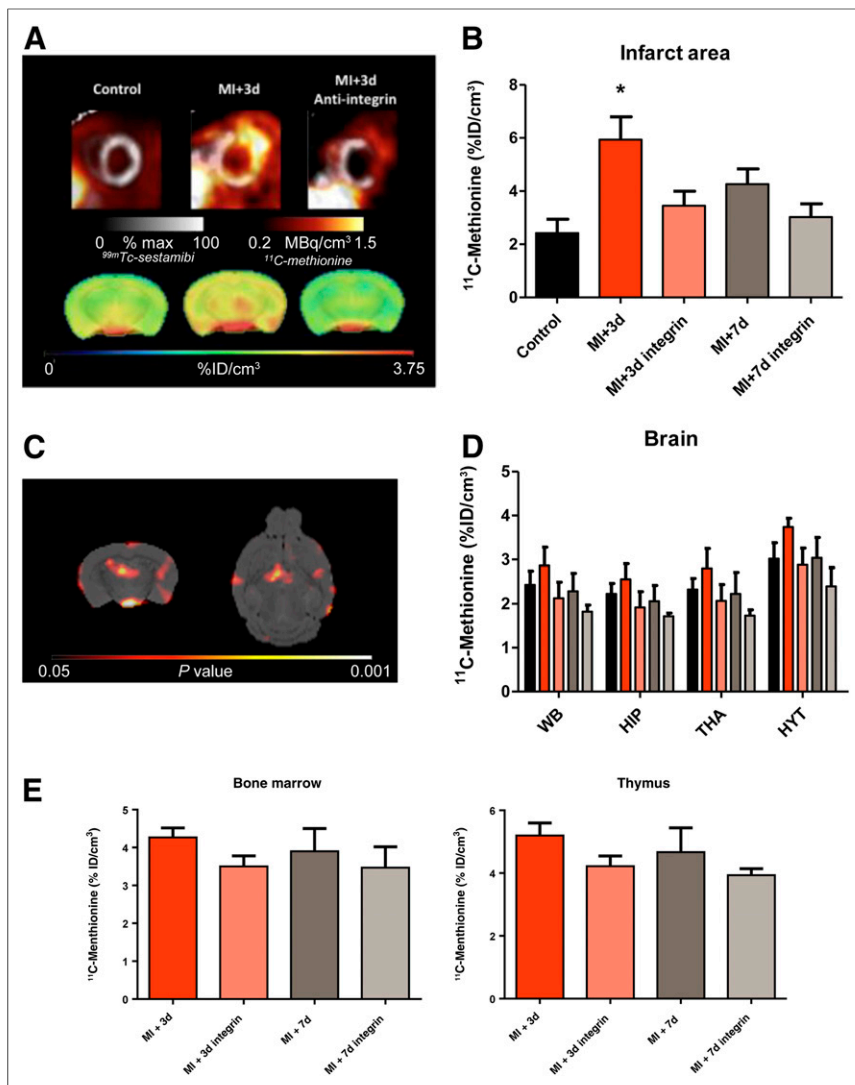**FIGURE 1.** ^{11}C-methionine uptake in heart and brain in control mice and after MI. (A) Representative cardiac and brain ^{11}C-methionine uptake are shown for control animals and 3 d after MI for untreated and treated animals. (B and D) Semiquantitative analysis of ^{11}C-methionine uptake shows increased uptake in infarct area (B) and brain regions (D) at 3 d after MI. (C) SPM t-map (Student's test distribution parametric map) identifies voxels that were significantly higher in animals 3 d after MI than control animals. (E) Semiquantitative analysis of ^{11}C-methionine uptake in hematopoietic organs (bone marrow and thymus) shows a comparably limited effect of antiintegrin treatment on these peripheral organs. *$P < 0.05$ compared with control. HIP = hippocampus; HYT = hypothalamus; THA = thalamus; WB = whole brain.

Image Analysis

Using PMOD software (version 3.7; PMOD Technologies), brain PET images were automatically coregistered to individual CT images, and the CT images were then fused to an MRI T2-weighted template (*14*). PET images were then coregistered to the MRI template, and a volume-of-interest template (*15*) was applied. Mean uptake normalized to the injected dose (percentage injected dose/cm^3) for each volume of interest was calculated. Cardiac and peripheral organ uptake (i.e., liver, bone marrow, and thymus) was analyzed using Inveon Research Workplace as previously described (*10*).

Immunohistochemistry

Untreated ($n = 8$) and antiintegrin-treated ($n = 8$) animals were sacrificed 3 and 7 d after MI. Brains were removed, snap-frozen, and

sliced in a cryostat (14 μm). Fluoroimmuno-histology targeting large neutral amino acid transporter (LAT-1) and either glial fibrillary acidic protein (GFAP) of astrocytes or CD68 or microglia was performed. Thawed brain sections were fixed in acetone, blocked with horse serum (10% in phosphate-buffered saline), and incubated with the primary antibodies (AlexaFluor488 anti-GFAP or AlexaFluor-488 anti-CD68 and AlexaFluor-647 antimouse CD98; Biolegend) for 60 min. Slides were then washed with phosphate-buffered saline, incubated with 4′,6-diamidino-2-phenylindole solution, and washed again, and a coverslip was applied using fluorescence mounting medium (FluoreGuard; Dianova). Brain slices were analyzed using an epifluorescence confocal microscope. Fluorescence signal for GFAP, CD68, and LAT-1 was quantified in dorsal hippocampus and thalamus.

Statistics

Differences in imaging studies were analyzed by nonparametric Kruskal–Wallis testing followed by post hoc testing with selected comparisons. Fluorescence immunostaining results were compared by 2-sided 2-sample t testing. Data are presented as mean ± SD. Differences were considered statistically significant at a P level of less than 0.05.

RESULTS

Serial PET demonstrated increased ^{11}C-methionine accumulation in the infarct territory at 3 d after MI, declining to the level of healthy controls by 7 d (Figs. 1A and 1B). A concomitant elevation of ^{11}C-methionine signal was evident in the whole brain at 3 d. This difference was reduced at 7 d, similarly to the heart (Figs. 1A and 1D). Statistical parametric mapping revealed the prominent signal increase in the hypothalamus, hippocampus, and dorsal thalamus regions (Fig. 1C). The systemic immune response was evident, with a modest elevation of ^{11}C-methionine accumulation in bone marrow and the thymus, reaching a maximum at 3 d after MI (Fig. 1E).

Pretreatment with antiintegrin antibody led to a significant decline in cardiac ^{11}C-methionine accumulation at 3 d (Figs. 1A and 1B). Uptake in the brain was comparably decreased, both in whole brain and in the regions of most pronounced elevation (Figs. 1A and 1D). Hepatic ^{11}C-methionine uptake was not affected by antiintegrin treatment (11.7 ± 2.0 vs. 10.9 ± 1.2 percentage injected dose/cm^3, P = NS), supporting interference with leukocyte extravasation over depletion. Overall, we found a good correlation between brain ^{11}C-methionine uptake and uptake in the MI territory ($r = 0.47$, $P < 0.05$).

Brain tissue immunostaining identified an elevated density of GFAP-positive astrocytes in the hippocampus at 3 d after MI, compared with integrin-treated animals (596 ± 141 vs. 350 ± 136;
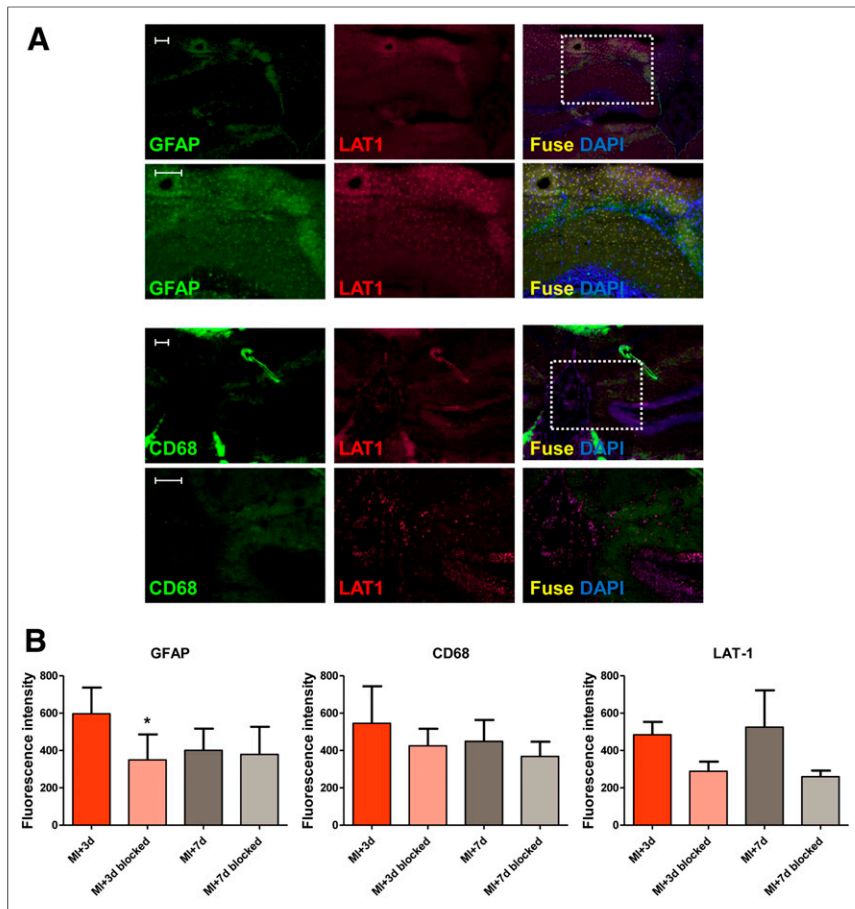
FIGURE 2. Immunostaining identifies astrocytes (GFAP), microglia (CD68), and amino acid transporter (LAT-1) in MI treated and untreated animals at 3 and 7 d. (A) Merged images show colocalization of LAT-1 and GFAP (upper 2 rows) but not with CD68 (lower 2 rows) in hippocampus 3 d after MI. Scale bar = 50 μm. (B) Semiquantitative analysis of GFAP, CD68, and LAT-1 fluorescence intensity in hippocampus. *$P < 0.05$ compared with control.

$P = 0.033$; Fig. 2). CD68-positive microglia were also present in the cortex around the hippocampus (Fig. 2). LAT-1 as the substrate for methionine uptake was visualized at 3 and 7 d after MI and was attenuated by antiintegrin treatment ($P = 0.052$, Fig. 2B). Of note, LAT-1 did not colocalize with CD68-positive microglia (Fig. 2A). Conversely, coimmunostaining demonstrated colocalization of LAT-1 with GFAP (Fig. 2A).

DISCUSSION

Recent studies have emphasized the interconnection between the heart and the brain after ischemic damage. In the present study, we expanded our prior observation of heart–brain inflammation networking using TSPO-targeted imaging, by using an alternative targeted radiotracer of inflammation, ^{11}C-methionine. We demonstrated that ^{11}C-methionine uptake is elevated in the brain early after MI. Moreover, we identified expression of the L-type amino acid transporter, particularly in GFAP-positive astrocytes, suggesting that ^{11}C-methionine identifies an astrocyte-driven component of neuroinflammation after acute MI, which is different from the microglia component analyzed by TSPO imaging in our prior work (7).

[11]C-methionine is widely used for glioma imaging and is suitable for imaging inflammatory conditions in the brain (9,16,17). We

and others reported selective accumulation of ^{11}C-methionine by proinflammatory leukocytes within the infarct region after acute MI (10,11). To our knowledge, the present study was the first to show that increased ^{11}C-methionine cardiac uptake is paralleled by increased brain uptake early after MI. Statistical parametric mapping points to the hippocampus as one the most affected regions, which is implicated in systemic inflammation and may lead to impaired neurogenesis and memory deficits (18,19). ^{18}F-FDG uptake in the amygdala has been suggested as a contributing factor to atherosclerotic plaque inflammation and major adverse cardiac events (20). Although quantitative analysis of murine amygdala is beyond the resolution of the PET camera, a tendency for increased amino acid metabolism was also identified in the present study.

Immunohistochemistry suggests increased LAT-1 in activated astrocytes but not CD68-positive microglia as the source of ^{11}C-methionine signal. This pattern is distinct from TSPO-ligand ^{18}F-GE180, which colocalized with microglia but not astroglia (7). The imaging time course suggests early neuroinflammatory astrocyte activity preceding microglia activation after MI, as methionine signal recovers to baseline at maximal microglial activation (7). Reactive astrocytes can be neurotoxic, producing reactive oxygen species and inflammatory cytokines. They also express high levels of amyloid precursor proteins (21). As such, MI-induced astrocytic activation may lead to amyloid-β production and further neuroinflammation, a vicious cycle that may promote Alzheimer disease pathology (22,23). Although modestly higher astrocyte staining could be regionally identified, both histology and PET imaging suggest a global brain response to MI. Statistical parametric mapping suggests preferential involvement of specific brain regions but requires dedicated regional analysis with higher-resolution techniques.

Application of an antiintegrin cocktail to inhibit cardiac leukocyte infiltration (10) also lowered brain ^{11}C-methionine uptake but did not affect other peripheral organs. Antiintegrin antibody therapy impairs the rolling and extravasation of neutrophils, monocytes, and macrophages, without a direct impact on leukocyte numbers (24). Similar to the PET signal, brain GFAP and LAT-1 were reduced, suggesting attenuated astrocyte activation, whereas CD68-positive microglia were unaffected. These findings suggest that astrocyte activation after MI is directly linked to infarct-induced inflammation and may point to proinflammatory cytokines as the cause of astrocytic activation. Neutrophils and proinflammatory monocytes, which exhibit high methionine uptake (10), appear to influence astrocyte activation. In contrast, peak microglial activation occurred slightly later (7) and did not decrease with the antiintegrin cocktail, suggesting that the microglia response is due to additional factors.

CONCLUSION

Methionine may delineate the astrocyte component of neuro-inflammation after MI, an ability which may be complementary to microglial imaging by TSPO-targeted tracers. The temporal profile of these distinct components may guide therapeutic interventions to improve neurologic outcomes after MI. Further dedicated studies are warranted to delineate the precise role of astrocytes in relation to microglial activation and cognitive impairment. Molecular imaging provides a multitracer toolbox to assess specific components of the heart–brain inflammatory axis.

DISCLOSURE

KEY POINTS

QUESTION: Can ^{11}C-methionine identify heart–brain inflammation networking after MI?

PERTINENT FINDINGS: Peak brain signal occurs on day 3 after MI, parallels peak myocardial inflammation, and is associated with activated astroglia (which is in contrast to previously used TSPO imaging that identifies microglia).

IMPLICATIONS FOR PATIENT CARE: Characterization of distinct immune–metabolic tissue patterns will help in the development of antiinflammatory, regenerative therapies.

REFERENCES

1. Breteler MM, Claus JJ, Grobbee DE, Hofman A. Cardiovascular disease and distribution of cognitive function in elderly people: the Rotterdam Study. *BMJ.* 1994;308:1604–1608.
2. Luchsinger JA, Reitz C, Honig LS, Tang MX, Shea S, Mayeux R. Aggregation of vascular risk factors and risk of incident Alzheimer disease. *Neurology.* 2005;65:545–551.
3. Qiu C, Winblad B, Marengoni A, Klarin I, Fastbom J, Fratiglioni L. Heart failure and risk of dementia and Alzheimer disease: a population-based cohort study. *Arch Intern Med.* 2006;166:1003–1008.
4. Nelson AR, Sweeney MD, Sagare AP, Zlokovic BV. Neurovascular dysfunction and neurodegeneration in dementia and Alzheimer's disease. *Biochim Biophys Acta.* 2016;1862:887–900.
5. de Roos A, van der Grond J, Mitchell G, Westenberg J. Magnetic resonance imaging of cardiovascular function and the brain: is dementia a cardiovascular-driven disease? *Circulation.* 2017;135:2178–2195.
6. Walker KA, Power MC, Gottesman RF. Defining the relationship between hypertension, cognitive decline, and dementia: a review. *Curr Hypertens Rep.* 2017;19:24.
7. Thackeray JT, Hupe HC, Wang Y, et al. Myocardial inflammation predicts remodeling and neuroinflammation after myocardial infarction. *J Am Coll Cardiol.* 2018;71:263–275.
8. Krstic D, Knuesel I. Deciphering the mechanism underlying late-onset Alzheimer disease. *Nat Rev Neurol.* 2013;9:25–34.
9. Glaudemans AW, Enting RH, Heesters MA, et al. Value of ^{11}C-methionine PET in imaging brain tumours and metastases. *Eur J Nucl Med Mol Imaging.* 2013;40:615–635.
10. Thackeray JT, Bankstahl JP, Wang Y, Wollert KC, Bengel FM. Targeting amino acid metabolism for molecular imaging of inflammation early after myocardial infarction. *Theranostics.* 2016;6:1768–1779.
11. Taki J, Wakabayashi H, Inaki A, et al. ^{14}C-methionine uptake as a potential marker of inflammatory processes after myocardial ischemia and reperfusion. *J Nucl Med.* 2013;54:431–436.
12. Kempf T, Zarbock A, Widera C, et al. GDF-15 is an inhibitor of leukocyte integrin activation required for survival after myocardial infarction in mice. *Nat Med.* 2011;17:581–588.
13. Langström B, Antoni G, Gullberg P, et al. Synthesis of L- and D-[methyl-^{11}C] methionine. *J Nucl Med.* 1987;28:1037–1040.
14. Ma Y, Hof PR, Grant SC, et al. A three-dimensional digital atlas database of the adult C57BL/6J mouse brain by magnetic resonance microscopy. *Neuroscience.* 2005;135:1203–1215.
15. Mirrione MM, Schiffer WK, Fowler JS, Alexoff DL, Dewey SL, Tsirka SE. A novel approach for imaging brain-behavior relationships in mice reveals unexpected metabolic patterns during seizures in the absence of tissue plasminogen activator. *Neuroimage.* 2007;38:34–42.
16. Hashimoto S, Inaji M, Nariai T, et al. Usefulness of [^{11}C]methionine PET in the differentiation of tumefactive multiple sclerosis from high grade astrocytoma. *Neurol Med Chir (Tokyo).* 2019;59:176–183.
17. Parente A, van Waarde A, Shoji A, et al. PET imaging with S-[^{11}C]methyl-L-cysteine and L-[methyl-^{11}C]methionine in rat models of glioma, glioma radiotherapy, and neuroinflammation. *Mol Imaging Biol.* 2018;20:465–472.
18. Chesnokova V, Pechnick RN, Wawrowsky K. Chronic peripheral inflammation, hippocampal neurogenesis, and behavior. *Brain Behav Immun.* 2016;58:1–8.
19. Murray C, Sanderson DJ, Barkus C, et al. Systemic inflammation induces acute working memory deficits in the primed brain: relevance for delirium. *Neurobiol Aging.* 2012;33:603–616.e3.
20. Tawakol A, Ishai A, Takx RA, et al. Relation between resting amygdalar activity and cardiovascular events: a longitudinal and cohort study. *Lancet.* 2017;389:834–845.
21. Frost GR, Li YM. The role of astrocytes in amyloid production and Alzheimer's disease. *Open Biol.* 2017;7:170228.
22. Rodriguez-Vieitez E, Saint-Aubert L, Carter SF, et al. Diverging longitudinal changes in astrocytosis and amyloid PET in autosomal dominant Alzheimer's disease. *Brain.* 2016;139:922–936.
23. Schöll M, Carter SF, Westman E, et al. Early astrocytosis in autosomal dominant Alzheimer's disease measured in vivo by multi-tracer positron emission tomography. *Sci Rep.* 2015;5:16404.
24. Li W, Nava RG, Bribriesco AC, et al. Intravital 2-photon imaging of leukocyte trafficking in beating heart. *J Clin Invest.* 2012;122:2499–2508.